














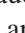






Transparent Optical-THz-Optical Link at 240/192 Gbit/s Over 5/115 m Enabled by Plasmonics

Yannik Horst , Tobias Blatter , Laurenz Kulmer , Bertold Ian Bitachon , Benedikt Baeuerle , Marcel Destraz , Wolfgang Heni , Stefan Koepfli , Patrick Habegger , Marco Eppenberger , Eva De Leo , Claudia Hoessbacher , Delwin L. Elder , Scott R. Hammond , Lewis E. Johnson , Larry R. Dalton , *Senior Member, IEEE*, Yuriy Fedoryshyn , Yannick Salamin , Maurizio Burla , *Senior Member, IEEE*, and Juerg Leuthold , *Fellow, IEEE*

(Post-Deadline Paper)

Abstract—A transparent Optical-subTHz-Optical link providing record-high single line rates of 240 Gbit/s and 192 Gbit/s on a single optical carrier over distances from 5 to 115 m is demonstrated. Besides a direct mapping of the optical to a 230 GHz subTHz-carrier frequency by means of a uni-traveling carrier (UTC) photodiode, we demonstrate direct conversion of data from the subTHz domain back to the optical domain by a plasmonic modulator. It is shown that the subTHz-to-optical upconversion can even be performed at good quality without any electrical amplifiers. Finally, at the receiver, the local oscillator is employed to directly map the optical signal back to the electrical baseband within a coherent receiver.

Index Terms—Microwave photonics, plasmonics, radio over fiber, silicon photonics, THz communications.

Manuscript received August 31, 2021; revised January 5, 2022 and January 28, 2022; accepted January 28, 2022. Date of publication February 4, 2022; date of current version March 16, 2022. This work was submitted for publication in IEEE Journal of Lightwave Technology (JLT) on 31 August 2021. This work was supported in part by the European Commission through the Horizon 2020 project ERC PLASILOR under Grant 670478, in part by the H2020 Project VERTIGO under Grant 822030, and in part by the Swiss National Fund Project Ambizione under Grant 173996. (*Corresponding author: Yannik Horst.*)

Yannik Horst, Tobias Blatter, Laurenz Kulmer, Bertold Ian Bitachon, Stefan Koepfli, Marco Eppenberger, Yuriy Fedoryshyn, Maurizio Burla, and Juerg Leuthold are with ETH Zurich, Institute of Electromagnetic Fields (IEF), 8092 Zurich, Switzerland (e-mail: yannik.horst@ief.ee.ethz.ch; tobias.blatter@ief.ee.ethz.ch; laurenz.kulmer@ief.ee.ethz.ch; bertold.bitachon@ief.ee.ethz.ch; stefan.koepfli@ief.ee.ethz.ch; marco.eppenberger@ief.ee.ethz.ch; yuriy.fedoryshyn@ief.ee.ethz.ch; maurizio.burla@ief.ee.ethz.ch; leuthold@ief.ee.ethz.ch).

Benedikt Baeuerle, Marcel Destraz, Wolfgang Heni, Patrick Habegger, Eva De Leo, and Claudia Hoessbacher are with Polariton Technologies Ltd., 8038 Zurich, Switzerland, and also with ETH Zurich, Institute of Electromagnetic Fields (IEF), 8092 Zurich, Switzerland (e-mail: benedikt@polariton.ch; marcel.destraz@polariton.ch; wolfgang@polariton.ch; patrick@polariton.ch; eva@polariton.ch; claudia@polariton.ch).

Delwin L. Elder, Scott R. Hammond, and Lewis E. Johnson are with the Nonlinear Materials Corporation, Queen Anne Ave North, Seattle, WA 98109 USA, and also with the University of Washington, Seattle, WA 98195-1700 USA (e-mail: delwinel@nonlinearmaterials.com; scotth@nonlinearmaterials.com; lewisj@nonlinearmaterials.com).

Larry R. Dalton is with the University of Washington, Seattle, WA 98195-1700 USA (e-mail: dalton@chem.washington.edu).

Yannick Salamin was with ETH Zurich, Institute of Electromagnetic Fields (IEF), 8092 Zurich, Switzerland. He is now with Research Laboratory of Electronics, MIT, Cambridge, MA 02139 USA (e-mail: salamin@mit.edu).

Color versions of one or more figures in this article are available at <https://doi.org/10.1109/JLT.2022.3148534>.

Digital Object Identifier 10.1109/JLT.2022.3148534

I. INTRODUCTION

HIGH-DATA-RATE subTHz wireless links can bridge optical links and will play an essential role in next generation mobile data networks. Fig. 1(a) shows some scenarios where subTHz links may overcome geographical obstacles or where a high-capacity link may be directly directed to a user. An advantage of subTHz carrier frequencies is the inherent capability to transmit highest capacities. In fact, subTHz capacities in the order of multiple 100s of Gbit/s will be needed to bridge a state-of-the-art optical link over a wireless channel [1]. Another advantage of subTHz carrier frequencies over, e.g., optical wireless links is the higher robustness against atmospheric turbulences [2] and visibility-limiting weather conditions such as fog [3], snow [4], haze [5], and dust [6].

In the past few years, an increasing number of wireless transmission demonstrations with line rates at and above 100 Gbit/s [7]–[18] for distances up to 20 m [7], a line rate of 132 Gbit/s over 110 m [16], and even a line rate of 300 Gbit/s over 0.5 m [11] have been reported. Even higher capacities of 600 Gbit/s [19] and up to 1056 Gbit/s [20] were achieved for distances of 2.8 m, and up to 3.1 m in combination with polarization multiplexing and/or MIMO schemes.

All of these successful subTHz transmission schemes have in common that they rely on direct optical-to-RF conversion schemes at the transmitter remote antenna unit (RAU). The conversion is thereby typically performed by a uni-traveling carrier (UTC) photodiode. The advantage of direct conversion from the optical to the RF by means of a photodiode lies in the large bandwidth offered by photonic technologies [21]. In fact, photonics allows manipulating RF signals at arbitrary frequencies using heterodyne mixing [22].

RF-to-optical conversion is subsequently needed at the receiver RAU. However, in all of the aforementioned experiments, the receiver typically relies on an electrical [23], [24] or optical [25] down-mixing of the THz signals to the baseband or an intermediate frequency, because no viable solution was available to directly encode the THz information onto an optical carrier. This electrical down-conversion is usually necessary as the received electrical signal is weak and a low noise amplification

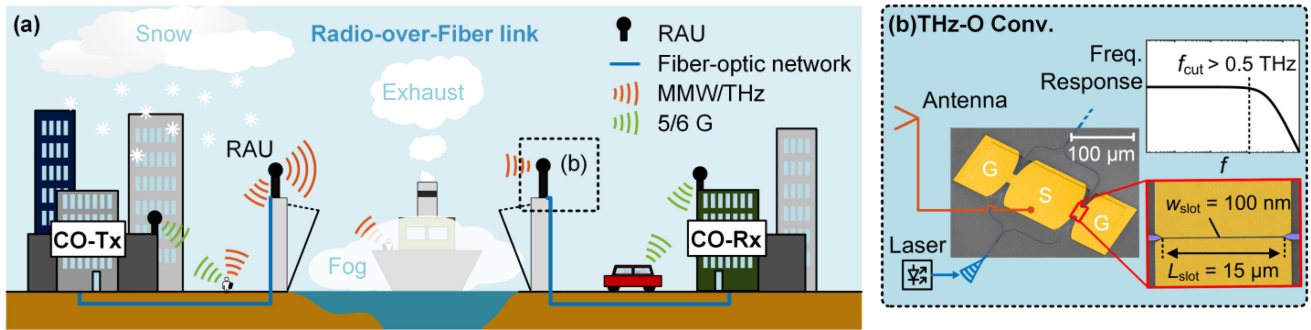


Fig. 1. (a) Vision of future communication networks, where THz links are transparently embedded in the fiber-optical network for backhauling and device-to-device applications. (b) Key technology for the THz-to-optical (back) conversion is a plasmonic Mach-Zehnder modulators that shows THz bandwidth, high sensitivity (no electrical amplification needed) and small footprint (active region: 100 nm x 15 μm). CO: central office; RAU: remote antenna unit; RoF: radio-over-fiber; Rx, receiver, Tx, transmitter.

stage is unavoidable. As a result, transmission experiments are confined to available electrical IF bandwidths in the order of 40 GHz. Also, in all of these experiments, the transmission is discontinued at the receiver RAU as a subsequent optical fiber stage would require an additional conversion back to the optical domain.

Yet, downconversion to the electrical domain can be avoided by directly mapping the RF signal into the optical domain using electro-optical (EO) modulators. Unfortunately, the modulators' bandwidth limits the accessible carrier frequencies to typical bandwidths below 80 GHz and with this the data rates [26]–[29]. In 2015, a new direct RF-to-optical conversion scheme relying on plasmonics was introduced [30]. In this approach, an RF signal is received by an on-chip antenna and converted to the optical domain by a seamless-integrated plasmonic modulator. The combination of a resonant antenna with gains of 10–20 dB and a field enhancement in the order of 30–40 dB was obtained when dropping off the antenna field across a slot within a plasmonic modulator. Enhancements in the order of 49 dB have already been shown [31]. As an advantage of this approach, it has been found that the received bandwidth is only limited by the design of the resonant antenna, but not the plasmonic modulator [30]–[33]. Plasmonic modulators, see Fig. 1(b), have already been reported to offer flat frequency responses beyond 500 GHz [34] and have been tested for operation up to 2.4 THz [35]. Therefore, the plasmonic modulator represents a perfect candidate for Radio-over-Fiber links with direct conversion at subTHz frequencies and beyond without bandwidth restrictions.

In this paper, we report on a record-high single optical carrier transparent data transmissions over a fiber-subTHz-fiber link with line rates of 240 Gbit/s over a short distance of 5 m and 192 and 150 Gbit/s over a medium distance of 115 m employing a plasmonic modulator. Transparency has been achieved by means of direct mapping of the subTHz signal onto the optical domain by a plasmonic modulator. Direct down-conversion to the electrical domain is performed by a coherent optical receiver. The subTHz-to-optical (THz-O) conversion scheme presented here is applicable to arbitrary carrier frequencies up to 500 GHz and beyond.

The content of the paper is an extended version of results first presented at the post-deadline session of the Optical Fiber Communications (OFC) conference 2021 [36].

II. EXPERIMENTAL CONFIGURATION

The experimental setup for demonstrating the optical-subTHz-optical link is illustrated in Fig. 2. It comprises a 6 km optical fiber span, a subsequent subTHz wireless link of 5 or 115 m lengths, and finally, an optical fiber link of up to 4 km. Key elements of the link are the optical-to-subTHz converter (O-THz Conv.) and the subTHz-to-optical converter (THz-O Conv.) on the RAUs which are both based on photonic technologies.

The components of the link are now described in more detail.

A. Central Office (CO) Optical Transmitter (Opt. Tx)

In the optical transmitter (Tx), an optical IQ modulator with a 3dB-bandwidth of 38 GHz maps a Nyquist frequency division multiplexed (FDM) [37] electrical data signal onto an optical carrier ($f_{c,Tx}$). The electrical data signal has been generated by a digital-to-analog converter (DAC) with an analog bandwidth of 40 GHz and 6 bits resolution. After the optical Tx, the data signal is transmitted through a 0...6 km standard single mode fiber (SSMF) span.

B. RAU Optical-to-subTHz Converter (O-THz Conv.)

At the optical-to-THz converter, the optical data signal is boosted by an erbium doped fiber amplifier (EDFA) and coupled to free-running laser detuned by the wireless carrier frequency $f_{THz} \sim 230$ GHz. The THz signal is situated in the 130 GHz wide window between 190 and 320 GHz that offers low atmospheric losses [38]. After power- and polarization alignment, the combined signals are fed to a UTC-PD, where the reference laser shifts the data to the THz domain, employing a heterodyne mixing scheme. The overall optical power entering the UTC-PD was between 8 and 14 dBm to provide THz output powers in the order of -25.5 to -13.4 dBm. After the UTC-PD, an off-shelf THz medium power amplifier (MPA) amplifies the THz data signal, delivering overall output powers of up to 10.6 dBm to the antenna. The MPA has a typical gain of 24 dB and a 70 GHz large-signal bandwidth. Schematics of the spectra of the signal before and after the O-THz Conv. are shown at points A and B in Fig. 2. In Fig. 5(c), the normalized output power of the O-THz converter (red curve) is plotted as a function of frequency between 0.1915 to 0.2705 THz. It illustrates the

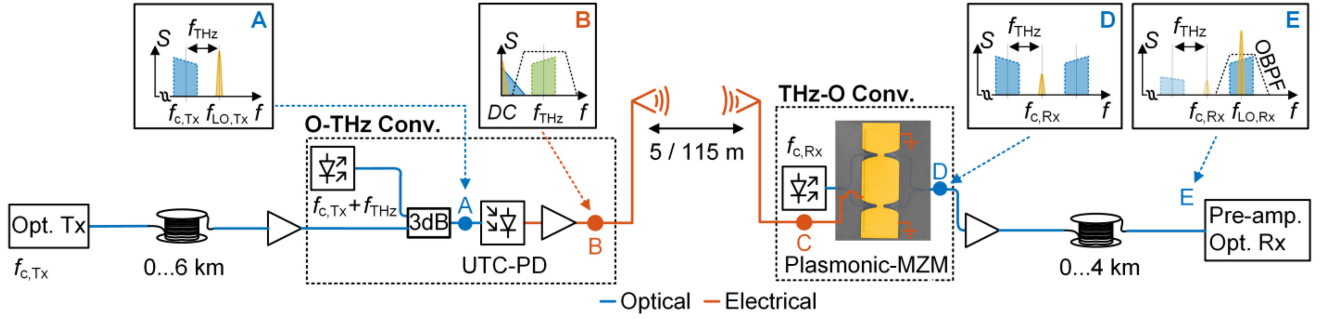


Fig. 2. Transparent fiber-THz-fiber link. First, the optical data signal is generated by encoding a signal onto an optical carrier $f_{c,Tx}$. The signal then propagates through a fiber span of 0...6 km and is fed to the optical-to-THz converter (O-THz Conv.), where it is mapped to the subTHz domain by heterodyne mixing in an ultra-fast uni-travelling carrier (UTC) photodiode using a cw local oscillator (see optical spectrums at points A and B). The THz data signal is amplified and emitted into the far-field by a directive THz antenna. Subsequently, it propagates over a free space distance of 5 m, respectively 115 m. At the THz-to-Optical converter (THz-O Conv.), the subTHz data signal is received by a second THz antenna and directly drives a plasmonic Mach Zehnder Modulator (without any additional amplification needed) and encodes the THz signal onto the optical carrier $f_{c,Rx}$. At this stage, the optical signal comprises of an upper and a lower sideband, as shown in point D. Subsequently, the optical signal is amplified by a low-noise EDFA. After fiber transmission, optical narrow band pass filters (OBPF) are used to suppress the optical carrier and to select one of the sidebands. In the coherent receiver (Rx), the signal is brought to the baseband by the local oscillator laser (optical frequency $f_{LO} = f_{c,Rx} + f_{THz}$) and offline digital signal processing is performed.

strong power variations of up to 15 dB over the considered frequency range of 79 GHz. Subsequently, Nyquist FDM data signal subcarriers were bit- and power-loaded. A total number N subcarriers were encoded and optimized to deliver the highest possible generalized mutual information (GMI). The GMI can be calculated by estimating the likelihood ratios using known data bits. It constitutes a good predictor for the achievable net-data rate after soft-decision forward error correction (FEC) [39].

Furthermore, using a single subcarrier, $N = 1$, we observed that the strong frequency variation of the O-THz converter leads to a performance penalty and thus, prevents successful transmission of symbol rates higher than 32 GBaud. Therefore, the usage of a Nyquist FDM was needed to transmit combined symbol rates of up to 75 GBaud across the THz link.

C. SubTHz Wireless Link of 5 m / 115 m

To test the potential of the transparent plasmonic fiber-to-subTHz-to-fiber transmission link, experiments were performed for two scenarios: A short range (5 m) and a medium range (115 m) scenario. At carrier frequencies around ~ 230 GHz, the free-space losses (FSPL) are 93.7 dB for 5 m and 120.9 dB for 115 m, respectively. To compensate for these high losses, off-the-shelf horn-antenna-lens configurations are used at the transmitter and receiver side for the 5 m link (see Fig. 3(a)). In the 115 m experiment, these are substituted by more directive antennas and a flat metal plate placed halfway. The metal plate thereby acts as a THz mirror to double the wireless link distance. The loss of the metal plate was measured to be 1–2 dB due to its imperfections (surface flatness, non-infinite size). The measured total link gain achieved with the THz antennas is 84.5 dB and 108.9 dB in the 5 m and 115 m link, respectively. Therefore, the transmission losses of the free-space (FS) sections equate to 9.2 dB and 12 dB.

D. RAU Subthz-To-Optical Converter (THz-O Conv.)

At the THz-O converter, the received THz data signal is directly guided from the antenna to a plasmonic Mach-Zehnder

modulator (MZM) [40] via a ground-signal-ground (GSG) RF probe. The device is fabricated on the silicon photonics (SiPh) platform, combining established SiPh-components with high-speed modulation offered by ultra-fast plasmonic phase modulators. The plasmonic modulator offers highest efficiency. An efficiency which has multiple reasons. For instance, there is an almost perfect overlap of the optical field with the electrical THz field [41], the nanometer-slot waveguide across which the THz field drops off or the slow-down effect of the plasmonic waveguide mode dispersion [42], [43]. As a result, the THz data signal is efficiently converted by the plasmonic modulator onto an optical carrier ($f_{c,Rx}$), without the need of any additional cost- and power-hungry electrical THz amplifiers. This direct THz-O conversion, see Fig. 3(a) and (b), is characterized by less complexity in comparison to alternative reception schemes [17], where the data signal is first down-converted to baseband by a THz mixer to be consequently again up-converted to optical domain by an EO modulator. In this work, mapping of the data signal to baseband is only performed at the final stage, in the Pre-Amp. Opt. Rx, see section II-E.

The induced phase modulation $\Delta\varphi$ in each arm of the plasmonic MZM is proportional to the field enhancement factor FE times the electrical RF/THz field [30], i.e.,

$$\Delta\varphi \propto FE \cdot E_{RF}(t) \quad (1)$$

with

$$FE = \sqrt{\frac{Z_d}{Z_0}} \sqrt{\frac{G_A}{4\pi}} \cdot \frac{\lambda_{RF}}{w_{slot}}, \quad (2)$$

where Z_d is the device impedance, Z_0 is the free-space impedance, G_A is the gain of the antenna, λ_{RF} is the wavelength of the electrical field and w_{slot} is the width of the plasmonic slot. While the first term depends on the chosen antenna and its gain, the second term is given by the plasmonic device with its nanometer small slot. For an effective wavelength $\lambda_{RF} = 0.4$ mm (vacuum wavelength $\lambda_{RF,0} = c/(230 \text{ GHz}) = 1.3$ mm) and $w_{slot} = 80$ –120 nm, the plasmonic modulator provides an

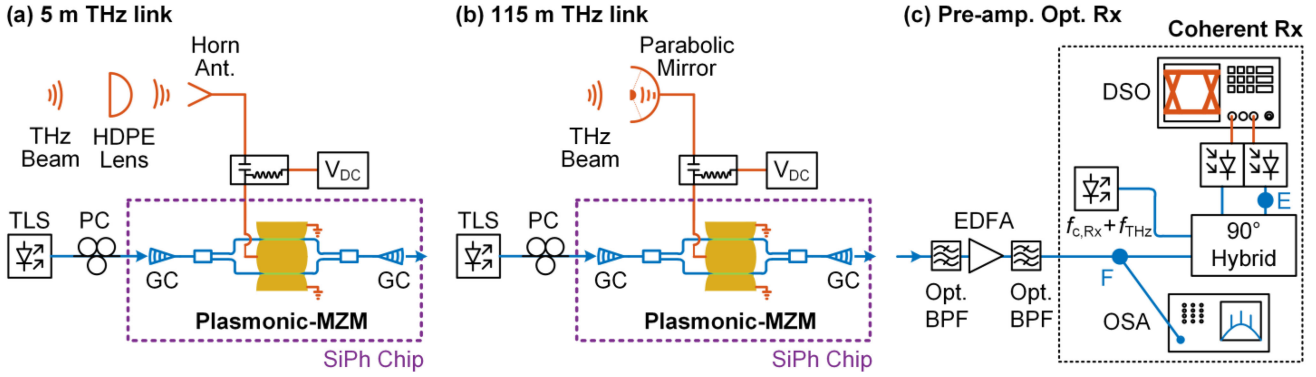


Fig. 3. Elements of the THz link in detail. THz-O Conv. with (a) a horn-antenna-lens configuration in the 5 m link and (b) a parabolic mirror in 115 m link, respectively. (c) Pre-amplified optical coherent receiver: Optical bandpass filters (Opt. BPF) are used to suppress the optical carrier and select one of the modulated sidebands. Afterwards, the optical signal is directly mapped to baseband by using a local oscillator laser (frequency $f_{LO} = f_{c,Rx} \pm f_{THz}$); DSO, digital sampling oscilloscope; EDFA, erbium doped fiber amplifier; HDPE, high density polyethylene; GC, grating coupler; OSA, optical spectrum analyzer; PC, polarization controller; SiPh, silicon photonics; TLS, tunable laser source.

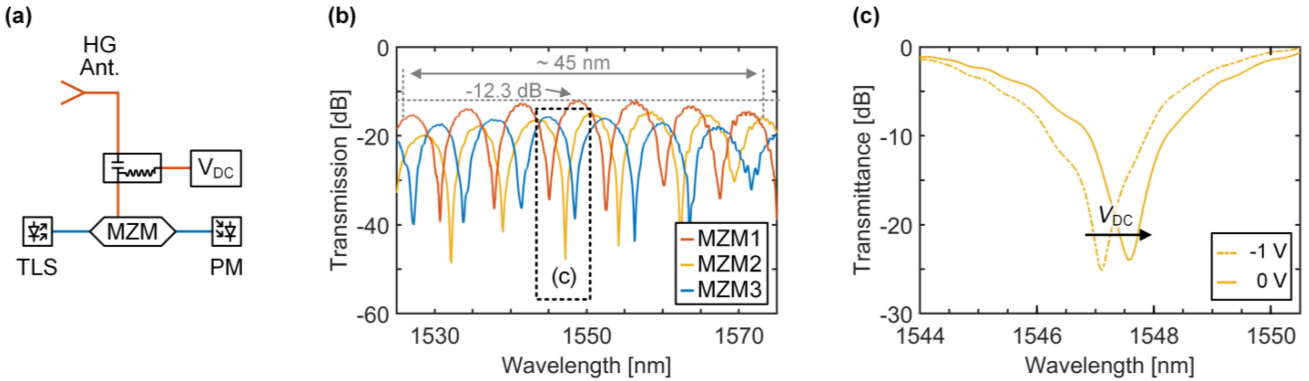


Fig. 4. (a) Setting the operation point in the THz-O converter by tuning the optical wavelength or voltage. (b) Transmission spectrum of the plasmonic modulators used in the THz experiments. The devices MZM1-3 featured 12.3 dB, 14.6 and 15.8 dB fiber-to-fiber-losses. The 3 dB bandwidth of the grating couplers is around 45 nm. (c) Voltage sweep method to determine the $V_{\pi}L$ of an MZM [44], [45]. Device MZM2 shows a $V_{\pi}L$ of 89 $V\mu\text{m}$, corresponding to $V_{\pi} = 8.9$ V for its slot length of 10 μm . HG, high gain; PM, power meter; TLS, tunable laser source.

enhancement in the order of 30 - 40 dB, eventually making an electrical amplification stage unnecessary.

The effective voltage drop across the slot is further increased by 3 dB, as the modulators are designed to be purely capacitive loads. The full reflection of the electrical wave at the end of the device results in a doubling of the 50 Ω -measured voltage [46]. The plasmonic MZM, operated in a push-pull configuration, is adjusted to the null point for amplitude modulation. A schematic of the resulting optical spectrum with a suppressed carrier and two modulated sidebands is depicted in point D of Fig. 2.

E. Central Office (CO) Pre-Amplified Optical Coherent Receiver (Pre-Amp. Opt. Rx)

The optical data signal is amplified by erbium-doped amplifiers (EDFA) and transmitted through a 0...4 km SSMF span, where one of the sidebands is selected by using optical bandpass filters (Opt. BPF), see Fig. 3(c). In the coherent receiver a narrow-linewidth laser, called local oscillator (LO), with an optical frequency of $f_{LO,Rx} = f_{c,Rx} + f_{THz}$ directly down-mixes the optical signal to the baseband. Finally, the electrical signal is

captured by a digital sampling oscilloscope (DSO). In contrast to direct detection schemes, where a complex signal needs to be down-mixed to an intermediate frequency, the requirements on bandwidth and sampling rate can be reduced by a factor of 2. The signal is then analyzed by an offline DSP stage consisting of Nyquist FDM demultiplexing, matched filtering, timing recovery, carrier and phase recovery, and linear equalization with 99 taps. The measured generalized mutual information (GMI) [39], bit-error-ratio (BER), and maximum net data rate after successful FEC decoding are used to evaluate the transmission performance.

III. EXPERIMENTAL RESULTS AND DISCUSSION

In this section, we describe the measured properties of the plasmonic modulator itself and then investigate the broadband performance of the 5 m (Exp. 1) and 115 m (Exp. 2 and 3) THz wireless transmission link achieved with the plasmonic modulators in the front-end THz receiver. Exp. 3 differs from Exp. 2 by placing an additional THz amplifier at point C in the THz-O converter.

Exp. 1: 5 m THz link – Line rate: 240 Gbit/s

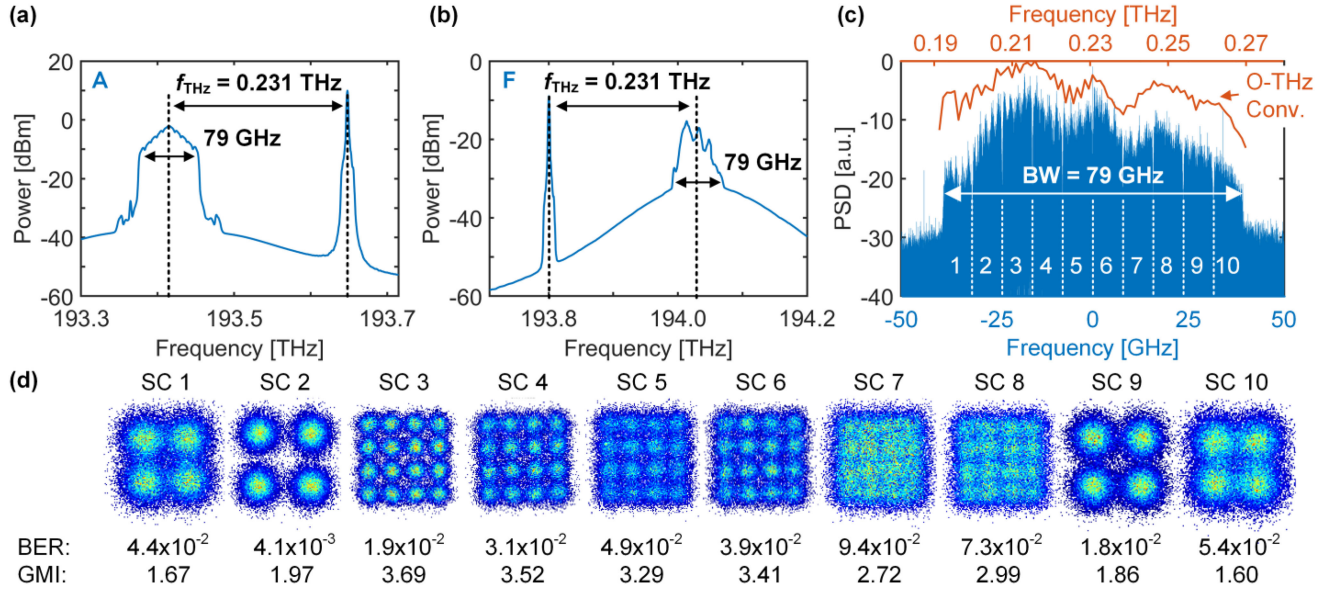


Fig. 5. Exp. 1: 5 m THz wireless data communication experiment with direct optical-to-THz and THz-to-optical conversion. (a) Optical spectrum measured at point A of the THz-O converter as shown in Fig. 2. The optical signal consists of a 75 Gbaud 10-Nyquist-FDM data signal with a bit-loading of [2, 2, 4, 4, 4, 4, 4, 4, 2, 2] bits/symbol at an optical frequency $f_{c,Tx}$ of 193.41 THz (1550 nm) and a local oscillator offset by $f_{THz} = 0.231$ THz. (b) Filtered and amplified optical spectrum before the 90°-Hybrid in the coherent optical receiver, see point F in Fig. 3(c). (c) Blue: digital received spectrum for the 75 Gbaud 10-Nyquist-FDM signal; red: frequency characteristic of the O-THz converter. (d) Constellation diagrams, the bit-error-ratios (BER) and measured generalized mutual information (GMI) of each subcarrier (SC) of the 75 Gbaud 10-Nyquist-FDM signal are shown, achieving a total net data rate of 200 Gbit/s, at a line rate of 240 Gbit/s. PSD, power spectral density.

A. High-Speed Plasmonic Modulator

In this work, the devices consist of two plasmonic phase shifters that are integrated into an imbalanced Mach-Zehnder Interferometer. The modulator is connected by GSG contacts, see Fig. 1(b), to directly apply the subTHz field over the two 10 to 15 μm plasmonic waveguide slots with widths of 100 nm. Due its asymmetric design, the operation point is either set by tuning the optical wavelength or by a DC bias over the slots, see Fig. 4(a). Alternatively, the devices feature thermo-optical phase shifters to set the operation point. These were not used though. For each experiment, the THz-to-optical plasmonic modulator has been tested for its performance. The fiber-to-fiber losses of the devices are 12.3 dB (MZM1), 14.6 dB (MZM2), and 16.1 dB (MZM3), in Exp. 3, 1, and 2, respectively. The losses include fiber-to-chip coupler losses L_{GC} of 2.9 - 3.5 dB per grating, photonic plasmonic converter losses L_{PPC} of 1 dB/converter, and plasmonic losses L_P of 0.45 - 0.55 dB/ μm . The corresponding transmission spectra are illustrated in Fig. 4(b). The MZMs feature extinction ratios exceeding 20 dB. By applying a DC voltage V_{DC} to the modulator's signal electrode, the optical spectrum can be shifted and the voltage-length product $V_{\pi}L$ can be measured [44], [45]. The devices show a high modulation efficiency with MZI $V_{\pi}L$ as low as 89 $\text{V}\mu\text{m}$, see Fig. 4(c). For an AC signal, the required voltage amplitude for a full on-off keying is consequently $V_P \sim 2.25$ V, given that the plasmonic modulator is operated as a purely capacitive load and has a slot length of 10 μm . From the $V_{\pi}L$, a nonlinear electro-optic coefficient of $r_{33} = 110 \text{ pmV}^{-1}$ can be derived. Another interesting number

is the achievable modulation index $\eta = V_{pp}/V_{\pi}$, where the peak-to-peak voltage is $V_{pp} = 2V_P$. As an example, we found with MZM2 in Exp. 1 a modulation index $\eta = 0.120$ for a THz input power of -1.5 dBm.

B. 5 m THz Wireless Link (Exp. 1)

Fig. 5. shows the 5 m data experiment results of Exp. 1. A 75 Gbaud 10-Nyquist-FDM digital data signal is generated in the offline Tx-DSP. All ten subchannels comprise periodically repeated sequence lengths of ~ 24500 symbols/channel and were bit-loaded with [2, 2, 4, 4, 4, 4, 4, 4, 2, 2] bits/symbol. Furthermore, all subcarriers were pulse-shaped by a square root raised cosine with a roll-off factor of 0.05 and equally spaced in frequency domain, so that each subcarrier had a symbol rate R_{sc} of 7.5 Gbaud. After conversion from digital to an analog baseband signal in the DAC, the data is modulated onto an optical carrier at frequency of 193.41 THz. The measured optical spectrum consisting of the optical data signal and the narrow-linewidth reference laser separated by $f_{THz} = 0.231$ THz are shown in Fig. 5(a). The total optical input power fed to the UTC-PD was around 14 dBm, leading to average output powers of approximately -13.4 dBm over the signal's bandwidth of 79 GHz. At the THz-to-optical converter, a 1545 nm optical carrier (13 dBm) is coupled to the SiPh chip. The THz field from the antenna ($V_{pp,50\Omega} = 0.532$ V, -1.5 dBm) is used to directly encode the data onto the light by means of the plasmonic MZM, making an electrical pre-amplification stage in the receiver negligible. Fig. 5(b) shows the selected (upper)

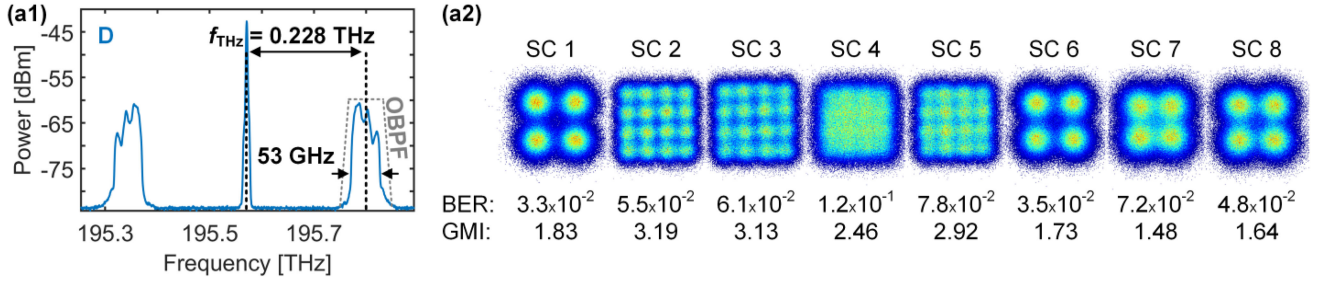
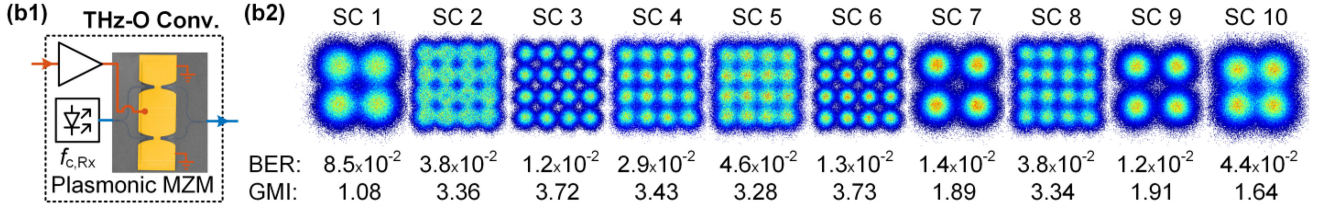
(a) Exp. 2: 115 m THz link – Driverless THz-O Converter – Line rate 150 Gbit/s**(b) Exp. 3: 115 m THz link – Driven THz-O Converter – Line rate 192 Gbit/s**

Fig. 6. Demonstration of 115 m THz wireless data communication experiment embedded in a fiber-optical network. (a) Rx-Driverless reception: (a1) At point D (see Fig. 2), measured optical spectrum consisting of its two sidebands and a suppressed carrier for an optical input power $P_{c,Rx}$ of 0 dBm. (a2) Constellation diagrams of each subcarrier (SC) of the 50 Gbaud 8-Nyquist-FDM signal with a bit-loading of [2, 4, 4, 4, 4, 2, 2, 2] bits/symbol are shown, achieving a total net data rate of 114.91 GBit/s at a line rate of 150 Gbit/s. (b) Rx-Driver reception: (b1) THz-O mixer scheme with electrical amplifier. (b2) Constellation diagrams of each subcarrier of the 60 Gbaud 8-Nyquist-FDM signal with a bit-loading of [2, 4, 4, 4, 4, 4, 2, 4, 2, 2] bits/symbol are shown, achieving a total net data rate of 164.38 GBit/s, at a line rate of 192 Gbit/s. GMI, generalized mutual information [bits/symbol].

sideband and the optical BPF-suppressed carrier. In Fig. 5(c), it can be clearly observed how the digital received signal (blue) follows the frequency dependency of the O-THz Conv. (red). Fig. 5(d) shows the constellation diagrams, BER, and GMI of each subchannel after performing offline DSP. The average net measured information rate of all subcarriers was measured to be 2.67 bits/symbol. At a line rate of 240 Gbit/s, this corresponds to a net rate of 200.25 Gbit/s. It has to be added that the DSP comprises a static T/2-spaced feed-forward equalizer (FFE) whose filter coefficients have been updated by a data-aided least mean square (LMS) with 1051 filter taps. Such a large number of linear taps were used to accurately model the THz channel and to derive the best possible signal quality. As a matter of fact, the number of taps can be reduced without significantly sacrificing performance. A T/2-spaced FFE with only 99 linear taps and decision-directed LMS updates leads to a capacity penalty of only 2%, i.e., the net-data rate reduces to 196.01 Gbit/s (~ 2.61 bits/symbol).

C. 115 m THz Wireless Link (Exp. 2 and 3)

Recalling our vision of communication networks (see Fig. 1), we observe that bridging FS distances of > 100 m will be needed. Therefore, we increased the THz wireless link distance from 5 m to 115 m. Furthermore, the optical-subTHz-optical span was extended by adding SSMF spans of 6 km and 4 km before and after, respectively, see Fig. 2. This was done for two main reasons. First, to demonstrate a realistic transparent fiber-wireless-fiber transmission link, where two COs are separated by several kilometers of optical fiber and occasionally bridged by > 100 m wireless subTHz links at optical capacities. Secondly, to show that Nyquist FDM enables channel-specific

bit-loading and reduces the complexity of the offline DSP due to its high chromatic dispersion (CD) tolerance. As the link losses increases by 3 dB, the symbol rate was reduced from 75 Gbaud to 50 Gbaud. Here, a total number of 8 subcarriers with a bit-loading of [2, 4, 4, 4, 4, 2, 2, 2] bits/symbol and an equally-spaced subsymbolrate of 6.25 Gbaud/channel was used. The THz carrier frequency f_{THz} was slightly shifted from 0.231 THz to 0.228 THz to achieve an overall higher output power of ~ 11.5 dBm after the O-THz converter. The measured optical spectrum directly after the plasmonic MZM with its two sidebands and suppressed carrier, at position D in Fig. 2, is displayed in Fig. 6(a1). The sidebands' frequency dependence has its origin in the bandwidth limitations of the transmitter components (DAC, driver, IQ modulator), see Fig. 5(a), and the transfer function of the O-THz Conv., see Fig. 5(c).

Fig. 6(a2) shows the measured constellation diagrams, BER and GMI of each subchannel. At a line rate of 150 Gbit/s, we achieved a net data rate of 114.91 Gbit/s, with an average GMI of all subcarriers of 2.29 bits/symbol. To demonstrate the CD resilience of Nyquist FDM, the same experiment was conducted without the SSMF spans. We obtained a comparable net data rate of 116 Gbit/s, at a line rate of 150 Gbit/s. This can be explained by the fact that effective symbol rate of each subcarrier R_{sc} is N times smaller than the total symbol rate R and, thus, the chromatic dispersion effect, which increases quadratically with the signal's bandwidth, was reduced by a factor of N^2 . In fact, the resulting CD tolerance was high enough so that no CD compensation algorithm was needed in the 115 m link.

Exp. 3: In a next step, we investigated the quality of our purely-passive plasmonic mixer by adding an active component to the THz-O Conv.: A second electrical THz amplifier with the same specifications was placed before the plasmonic MZM, see

TABLE I
PLASMONIC ENHANCEMENT VS. ELECTRICAL AMPLIFICATION

	Symbol rate [Gbaud]	Line rate [Gbaud]	GMI ^a [bits/symbol]
With THz Amp.	60	192	2.74
Without THz Amp.	50	150	2.29

^aGMI = generalized mutual information.

point C in Fig. 6(b1). The total optical power into the UTC-PD was decreased by 7 dB to not oversaturate the second amplifier. The plasmonic MZM was driven by a 6.5 dBm THz data signal ($V_{pp,50\Omega} = 1.34$ V), and a hollow-waveguide-based variable attenuator was used to protect the output port of the amplifier from reflections of the device. To optimize the measured total information rate, a 60 Gbaud 10-Nyquist-FDM signal was bit- and power-loaded in the digital domain. Each subcarrier's measured constellation diagram, BER and GMI is plotted in Fig. 6(b2). For the total line rate of 192 Gbit/s of all 10 subchannels, an average GMI of 2.74 bits/symbol was measured, resulting in a net data rate of 164.38 Gbit/s.

The electrical amplifier at the THz receiver does provide an increase in the data-rate. Yet, the overall advantage is moderate (see Table I). While the quality of the inner subcarriers can be improved (compare constellation diagrams of Fig. 6(a2) and (b2)), the outer subcarriers' performance remained unchanged. Consequently, the symbol rate could be increased by 20%, which is low given the fact that the THz signal driving the plasmonic MZM was increased by 8 dB. This can be explained considering that the bandwidth of the THz link is further decreased by the additional BW-limitations of the second THz amplifier. In contrast, in the 5 m THz link, where no second THz amplifier was used, higher symbol rates of up to 75 Gbaud have been achieved. This demonstrates that the photonic THz-O converter, i.e., the plasmonic MZM, introduces no bandwidth limitations to the system. The achievable symbol rates are firstly limited by the O-THz converter and secondly by the optical transmitter, i.e., DAC and IQ modulator. In the 5 m link, the performance was mainly limited by amplified spontaneous emission (ASE) noise of the first EDFA after the Plasmonic MZM. Experiments showed that the SNR linearly increases with the optical power in the modulated sideband(s). In future THz links, the achievable data rates might be increased by further improving the efficiency of THz-O conversion. This can be done by either co-integration of the plasmonic modulator with the subTHz antenna or by improvement of the device performance itself.

IV. CONCLUSION

In this work we have demonstrated the first transparent fiber-THz-fiber link at RF frequencies higher than 200 GHz achieving record-high optical single carrier data rates. Transparency is enabled by a plasmonic modulator with its >500 GHz bandwidth capable of mapping the THz signal onto an optical carrier. In a first experiment, the link was tested for its performance over a FS distance of 5 m achieving a line rate of 240 Gbit/s and net data rate of 200.25 Gbit/s. In a second experiment, the

wireless THz link distance was increased to 115 m and complemented by a 6 km and 4 km fiber. Despite the 10-fold distance increase, the high sensitivity of the plasmonic mixer towards THz frequencies enabled data transmissions at line rates of 150 Gbit/s and net-data rates of up to 114.9 Gbit/s, all accomplished without any electrical amplification at the receiving THz-O Converter. Adding a THz amplifier to the THz-O Converter allows to increase the achievable data rates. With the amplifier, line rates of 192 Gbit/s and net-data rates of 164.4 Gbit/s net rates were found. These data-rate improvements are moderate though. Electronic bandwidth limitations of the amplifier have limited a further data-rate increase. The experiments illustrate that driverless THz-O schemes based on a simple plasmonic modulator offer are attractive and indeed enable the realization of future transparent high-capacity fiber-wireless links. Furthermore, its compact footprint fabricated on a Si photonic platform enables scalability at low costs and complexity.

ACKNOWLEDGMENT

We thank NTT Electronics for the UTC-PD. We thank Cleanroom Operations Teams of the Binnig and Rohrer Nanotechnology Center (BRNC) for their help and support.

REFERENCES

- [1] T. Nagatsuma, "Advances in terahertz communications accelerated by photonics technologies," in *Proc. 24th OptoElectron. Commun. Conf.*, 2019, pp. 1–3.
- [2] J. Ma, L. Moeller, and J. Federici, "Experimental comparison of terahertz and infrared signaling in controlled atmospheric turbulence," *J. Infrared, Millimeter, Terahertz Waves*, vol. 36, no. 2, pp. 130–143, 2015.
- [3] Y. Yang, M. Mandehgar, and D. R. Grischkowsky, "Broadband THz signals propagate through dense fog," *IEEE Photon. Technol. Lett.*, vol. 27, no. 4, pp. 383–386, Feb. 2015.
- [4] Y. Amarasinghe, W. Zhang, R. Zhang, D. M. Mittleman, and J. Ma, "Scattering of terahertz waves by snow," *J. Infrared, Millimeter, Terahertz Waves*, vol. 41, no. 2, pp. 215–224, 2020.
- [5] Q. Jing, D. Liu, and J. Tong, "Study on the scattering effect of terahertz waves in near-surface atmosphere," *IEEE Access*, vol. 6, pp. 49007–49018, 2018.
- [6] K. Su, L. Moeller, R. B. Barat, and J. F. Federici, "Experimental comparison of terahertz and infrared data signal attenuation in dust clouds," *J. Opt. Soc. Amer. A*, vol. 29, no. 11, pp. 2360–2366, 2012.
- [7] S. Koenig *et al.*, "Wireless sub-THz communication system with high data rate," *Nature Photon.*, vol. 7, no. 12, 2013, Art. no. 977.
- [8] H. Shams *et al.*, "100 Gb/s multicarrier THz wireless transmission system with high frequency stability based on a gain-switched laser comb source," *IEEE Photon. J.*, vol. 7, no. 3, Jun. 2015, Art. no. 7902011.
- [9] T. Nagatsuma *et al.*, "Real-time 100-Gbit/s QPSK transmission using photonics-based 300-GHz-band wireless link," in *Proc. IEEE Int. Topical Meeting Microw. Photon.*, 2016, pp. 27–30.
- [10] X. Yu *et al.*, "160 Gbit/s photonics wireless transmission in the 300–500 GHz band," *APL Photon.*, vol. 1, no. 8, 2016, Art. no. 081301.
- [11] X. Pang *et al.*, "260 Gbit/s photonic-wireless link in the THz band," in *Proc. IEEE Photon. Conf.*, 2016, pp. 1–2.
- [12] X. Pang *et al.*, "Single channel 106 Gbit/s 16QAM wireless transmission in the 0.4 THz band," in *Proc. Opt. Fiber Commun. Conf.*, 2017, Paper Tu3B.5.
- [13] V. K. Chinni *et al.*, "Single-channel 100 Gbit/s transmission using III–V UTC-PDs for future IEEE 802.15.3d wireless links in the 300 GHz band," *Electron. Lett.*, vol. 54, no. 10, pp. 638–640, 2018.
- [14] A. Udalcovs *et al.*, "107.1-Gbps net-rate transmission over a joint 51km-fibre-and-10.7 m-wireless link for terahertz radio access networks," in *Proc. 45th Eur. Conf. Opt. Commun.*, 2019, pp. 1–4.
- [15] X. Li *et al.*, "132-Gb/s photonics-aided single-carrier wireless terahertz-wave signal transmission at 450GHz enabled by 64QAM modulation and probabilistic shaping," in *Proc. Opt. Fiber Commun. Conf. Exhibit.*, 2019, pp. 1–3.

- [16] T. Harter *et al.*, “Generalized Kramers–Kronig receiver for coherent terahertz communications,” *Nature Photon.*, vol. 14, no. 10, pp. 601–606, 2020.
- [17] C. Castro, R. Elschner, T. Merkle, C. Schubert, and R. Freund, “100 Gb/s real-time transmission over a THz wireless fiber extender using a digital-coherent optical modem,” in *Proc. Opt. Fiber Commun. Conf.*, 2020, Paper M4I.2.
- [18] J. Tebart, M. Steeg, F. Exner, A. Czulwik, and A. Stöhr, “Frequency-Scalable coherent radio-over-fiber architecture for 100 Gbit/s wireless transmission,” *URSI Radio Sci. Lett.*, vol. 2, pp. 1–5, 2020.
- [19] S. Jia *et al.*, “ 2×300 Gbit/s line rate PS-64QAM-OFDM THz photonic-wireless transmission,” *J. Lightw. Technol.*, vol. 38, no. 17, pp. 4715–4721, Sep. 2020.
- [20] X. Li *et al.*, “1-Tb/s millimeter-wave signal wireless delivery at D-band,” *J. Lightw. Technol.*, vol. 37, no. 1, pp. 196–204, Jan. 2019.
- [21] T. Nagatsuma *et al.*, “Terahertz wireless communications based on photonics technologies,” *Opt. Exp.*, vol. 21, no. 20, pp. 23736–23747, 2013.
- [22] T. Nagatsuma, H. Ito, and T. Ishibashi, “High-power RF photodiodes and their applications,” *Laser Photon. Rev.*, vol. 3, no. 1–2, pp. 123–137, 2009.
- [23] C. Jastrow *et al.*, “Wireless digital data transmission at 300 GHz,” *Electron. Lett.*, vol. 46, no. 9, pp. 661–663, 2010.
- [24] I. Kallfass *et al.*, “Towards MMIC-based 300 GHz indoor wireless communication systems,” *IEICE Trans. Electron.*, vol. 98, no. 12, pp. 1081–1090, 2015.
- [25] T. Harter *et al.*, “Wireless THz link with optoelectronic transmitter and receiver,” *Optica*, vol. 6, no. 8, pp. 1063–1070, 2019.
- [26] A. J. Seeds, H. Shams, M. J. Fice, and C. C. Renaud, “Terahertz photonics for wireless communications,” *J. Lightw. Technol.*, vol. 33, no. 3, pp. 579–587, Feb. 2015.
- [27] C. Yang, X. Li, J. Xiao, N. Chi, and J. Yu, “Fiber-wireless integration for 80 Gbps polarization division multiplexing–16QAM signal transmission at W-band without RF down conversion,” *Microw. Opt. Technol. Lett.*, vol. 57, no. 1, pp. 9–13, 2015.
- [28] T. P. McKenna, J. A. Nanzer, and T. R. Clark, “Photonic downconverting receiver using optical phase modulation,” in *Proc. IEEE MTT-S Int. Microw. Symp.*, 2014, pp. 1–3.
- [29] P. T. Dat *et al.*, “Transparent fiber–radio–fiber bridge at 101 GHz using optical modulator and direct photonic down-conversion,” in *Proc. Opt. Fiber Commun. Conf. Exhibit.*, 2021, pp. 1–3.
- [30] Y. Salamin *et al.*, “Direct conversion of free space millimeter waves to optical domain by plasmonic modulator antenna,” *Nano Lett.*, vol. 15, no. 12, pp. 8342–8346, 2015.
- [31] Y. Salamin *et al.*, “Microwave plasmonic mixer in a transparent fibre-wireless link,” *Nature Photon.*, vol. 12, no. 12, pp. 749–753, 2018.
- [32] S. Ummethala *et al.*, “THz-to-optical conversion in wireless communications using an ultra-broadband plasmonic modulator,” *Nature Photon.*, vol. 13, no. 8, pp. 519–524, 2019.
- [33] Y. Salamin *et al.*, “300 GHz plasmonic mixer,” in *Proc. Int. Topical Meeting Microw. Photon.*, 2019, pp. 1–4.
- [34] M. Burla *et al.*, “500 GHz plasmonic Mach-Zehnder modulator enabling sub-THz microwave photonics,” *APL Photon.*, vol. 4, no. 5, 2019, Art. no. 056106.
- [35] Y. Salamin *et al.*, “Compact and ultra-efficient broadband plasmonic terahertz field detector,” *Nature Commun.*, vol. 10, no. 1, 2019, Art. no. 5550.
- [36] Y. Horst *et al.*, “Transparent optical-THz-optical link transmission over 5/115 m at 240/190 Gbit/s enabled by plasmonics,” in *Proc. Opt. Fiber Commun. Conf. Exhibit.*, 2021, pp. 1–3.
- [37] R. Schmogrow *et al.*, “Nyquist frequency division multiplexing for optical communications,” in *Proc. CLEO: Sci. Innov.*, 2012, Paper CTh1H.2.
- [38] International Telecommunication Union, *ITU-R P.676-6, Attenuation by Atmospheric Gases*, ITU, 2005.
- [39] A. Alvarado, E. Agrell, D. Lavery, R. Maher, and P. Bayvel, “Replacing the soft-decision FEC limit paradigm in the design of optical communication systems,” *J. Lightw. Technol.*, vol. 33, no. 20, pp. 4338–4352, Oct. 2015.
- [40] W. Heni *et al.*, “108 Gbit/s plasmonic Mach-Zehnder modulator with >70-GHz electrical bandwidth,” *J. Lightw. Technol.*, vol. 34, no. 2, pp. 393–400, Jan. 2016.
- [41] A. Melikyan *et al.*, “High-speed plasmonic phase modulators,” *Nature Photon.*, vol. 8, no. 3, pp. 229–233, 2014.
- [42] C. Haffner *et al.*, “All-plasmonic Mach-Zehnder modulator enabling optical high-speed communication at the microscale,” *Nature Photon.*, vol. 9, no. 8, 2015, Art. no. 525.
- [43] C. Haffner *et al.*, “Plasmonic organic hybrid modulators—Scaling highest speed photonics to the microscale,” *Proc. IEEE*, vol. 104, no. 12, pp. 2362–2379, Dec. 2016.
- [44] W. Heni *et al.*, “Nonlinearities of organic electro-optic materials in nanoscale slots and implications for the optimum modulator design,” *Opt. Exp.*, vol. 25, no. 3, pp. 2627–2653, 2017.
- [45] A. Melikyan *et al.*, “Plasmonic-organic hybrid (POH) modulators for OOK and BPSK signaling at 40 Gbit/s,” *Opt. Exp.*, vol. 23, no. 8, pp. 9938–9946, 2015.
- [46] W. Heni *et al.*, “Plasmonic IQ modulators with attojoule per bit electrical energy consumption,” *Nature Commun.*, vol. 10, no. 1, 2019, Art. no. 1694.